NENE
International Conference
Nuclear Energy for New Europe

SUB-CHANNEL ANALYSIS OF THE MYRRHA REACTOR WITH OPENFOAM: NUMERICAL ASSESSMENT OF TURBULENCE MODELS

Martina Di Gennaro
Politecnico di Milano, Department of Energy, Nuclear Engineering Division
Via la Masa, 34/A
I-20156, Milano, Italy
martina.digennaro@polimi.it

ABSTRACT

The heavy liquid metal Lead-Bismuth Eutectic (LBE) is the primary coolant of the MYRRHA reactor, chosen because of its high heat removal capability, low melting point, non-violent reactivity to water and low neutron absorption. One of the phenomena to be considered for the operation of the reactor with LBE-coolant is the erosion/corrosion of the fuel pin cladding. For this reason, it is key to provide accurate estimations of the cladding outer temperature and LBE velocity during operation. In this work, I investigate the thermal-hydraulic behaviour of LBE in the MYRRHA IPS sub-channel (i.e., In-Pile test Section, core design version 1.8), with the perspective of constructing boundary conditions for fuel pin thermo-mechanical analyses. One of the main challenges in the numerical simulation of liquid metals flows with low Prandtl number (~ 0.025 for LBE) is to establish a reliable turbulent heat transfer modelling, not being possible to rely on the Reynolds analogy based on the direct proportionality between momentum and thermal boundary layers. A comparative study of different turbulence models is presented for studying the low-Prandtl turbulent flow of LBE in the MYRRHA hexagonal rod bundle characterized by a pitch-to-diameter ratio of 1.28. To this end, the Reynolds-Average Simulation (RAS) models available in the open-source fluid dynamics software OpenFOAM have been applied and compared with each other. The comparison focuses on key thermal-hydraulic parameters, such as the sub-channel temperature field, velocity field, pressure drops, and Nusselt number during reactor normal operation.

1 INTRODUCTION

Lead-Bismuth Eutectic (LBE) as nuclear coolant material was primarily studied in the former Soviet Union for use in alpha-class nuclear submarines during the Cold War. In view of its high heat removal capability, low melting point, non-violent reactivity to water and low neutron absorption, LBE is considered a promising coolant material and a suitable high-power spallation neutron target for the MYRRHA (Multi-purpose hYbrid Research Reactor for High-tech Applications) Accelerator-Driven System (ADS), approaching the licensing process in Belgium [1, 2]. A key issue in the development of MYRRHA is the compatibility of structural materials with LBE, in particular in terms of the erosion / corrosion mechanism of the fuel pin cladding, especially at elevated cladding outer temperature and coolant velocity.

Computational Fluid Dynamics (CFD) codes can be used to provide high-fidelity estimations of these thermal-hydraulic parameters during reactor operation. Compared to ordinary fluids with Prandtl number around one (water and air), LBE with two order of magnitude lower

Prandtl number, ~ 0.025, show significantly different behaviours. At such a low Prandtl number, the thermal boundary layer is much thicker than the hydraulic boundary layer therefore the numerical treatment of the boundary layer near the heated walls needs special care not being possible to rely on the Reynolds analogy [3].

Moreover, some works indicate that the liquid metals flow in the fuel bundles is three-dimensional and exhibits coherent structures which cause mixing and may also lead to structure vibrations [4]. In order to support the core design, a numerical method able to capture these phenomena and correctly predict the heat transport in the fuel rod bundle is necessary.

The purpose of the current analysis is to perform a comparative study of different URANS (Unsteady Reynolds-average Navier-Stokes) turbulence models available in the open-source fluid dynamics software OpenFOAM (version 6.0) [5], to investigate the primary coolant flow behaviour in the interior sub-channel of the MYRRHA In-Pile test Section (IPS) sub-assembly (core design version 1.8) during a normal irradiation scenario.

A brief description of the MYRRHA subcritical core configuration is provided in Section 2. Then, Section 3 focuses on the main aspects of the sub-channel analyses performed in OpenFOAM. The qualitative and quantitative results obtained are presented and discussed in Section 4. Conclusions are drawn in Section 5.

2 MYRRHA SUBCRITICAL CORE CONFIGURATION

Current research on MYRRHA focuses on the subcritical core configuration coupled to an accelerator-driven system, which foresees a thermal power output of 70 MWth produced among 78 hexagonal Fuel Assemblies (FAs) (Figure 1). Each fuel assembly consist of 127 wire-wrapped cylindrical fuel elements loaded with a U-Pu-Am mixed oxide (Am-MOX) fuel encased within the DIN 1.4970 cladding (15-15Ti stainless steel family).

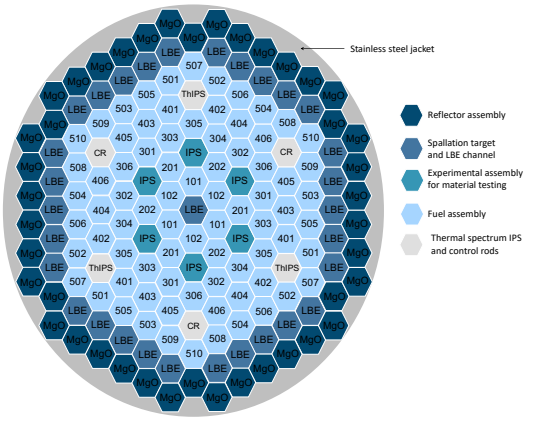

Figure 1: Radial view of the MYRRHA subcritical core layout according to the current design “Revision 1.8”.

The 78 FAs are grouped in batches and their subdivision into batches follows the core 1/3rd azimuthal symmetry around the central assembly, making each batch be composed of three FAs [6]. A typical MYRRHA operating schedule consists of irradiation cycles: each fuel assembly spends about 90 Effective Full Power Days (EFPDs) in a specific batch of the core followed by 30 days of shutdown for core reshuffling, loading and maintenance [7].

The focus of the analyses performed in this work is the single-cycle IPS positioned in the second concentric ring of the core (around the central spallation target) and dedicated to material testing and experimental irradiation with fast neutron fluxes of innovative fuel pins fuelled e.g., with Am-MOX fuel. In particular, here I refer to the hottest Am-MOX pin identified as the pin placed in the harshest position (in terms of boundary conditions and temperature) within the fuel assembly and characterized by an integral power produced of 9012 W.

3 NUMERICAL SETUP

3.1 Geometric description of the coolant domain

Figure 2 reports a sketch of the hexagonal rod bundle of the IPS sub-assembly characterized by a pitch-to-diameter ratio of 1.28 and a pin active height equal to 650 mm. The analysis

was carried out on the interior coolant sub-channel without considering the presence of the pin wire-wrapper and preserving the original flow passage area, 12.5 mm^2, with a mass flow rate of 0.24 kg s^{-1}. Due to the symmetry only 1/3 sub-channel is considered as computational domain, with an hydraulic diameter of 4.86 mm. The mesh generation process was handled with ANSYS Workbench 2023 R1. After a grid independence study, performed using the coolant temperature as reference output, the finer mesh (mesh number four in Table 1 with fully resolved grid) has been selected for the analysis in this work in order to have a good resolution of the boundary layer. The total length of the meshed channel corresponds to the pin active height plus an additional non-heated zone of 100 mm at the bottom, in order to obtain a hydraulically developed flow (Figure 3), and an additional buffer zone of 100mm at the top in order to prevent outlet boundary inconsistencies.

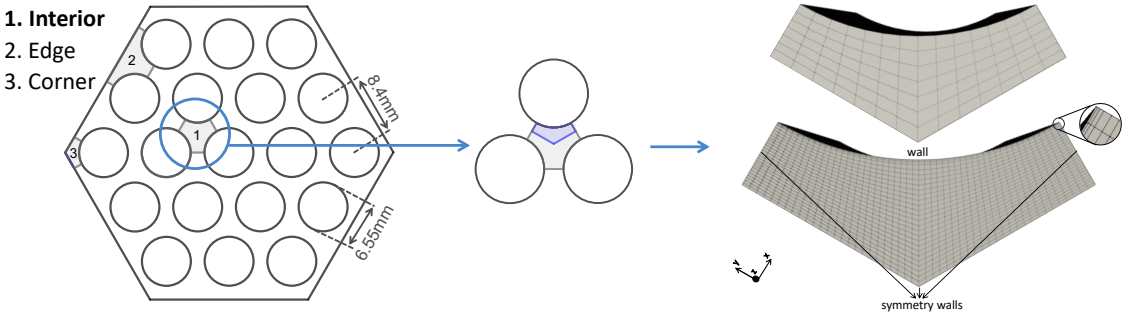

Figure 2: Sketch of the IPS sub-assembly and the zoom on the interior sub-channel with the considered computational domain highlighted in blue (left and center). On the right, the coarser (top) and the finer (bottom) meshes of the coolant domain adopted for the grid independence study are shown (Table 1).

Table 1: Main characteristics of the discrete grids employed for the mesh independency study. The mesh 4 is the one selected for the analysis performed in this work.

	Hexaedral elements	Aspect ratio	Max non-orthogonality	Max skewness	Average y^+	axial elements	Wall layers
Mesh 1	29'400	45.96	26	0.73	40	300	0
Mesh 2	60'000	32.92	27	0.75	30	300	0
Mesh 3	240'000	65.98	28	0.77	9	300	0
Mesh 4	405'000	743.73	29	0.78	~ 1	300	3

3.2 Governing equations and numerical methods

Under the assumption of incompressible fluid, the dynamics of the LBE flow is described by the Navier-Stokes equations coupled with the energy equation under the Boussinesq[1] approximation for density:

$$\begin{cases} \dfrac{\partial \mathbf{u}}{\partial t} + (\mathbf{u}\cdot\nabla)\mathbf{u} - \nabla\cdot(\nu\nabla\mathbf{u}) = -\dfrac{1}{\rho}\nabla p - \mathbf{g}\beta(T - T_{ref}) \\ \nabla\cdot\mathbf{u} = 0 \\ \dfrac{\partial T}{\partial t} + \mathbf{u}\cdot(\nabla T) = -\nabla\cdot(-\alpha\nabla T) \end{cases} \tag{1}$$

[1] It assumes that density variations are linear with temperature and play a role only in the buoyancy term.

where **u** is the velocity vector, ν is the kinematic viscosity of the fluid, p is the pressure, **g** is the gravity acceleration, β is the thermal expansion coefficient of the fluid, T is the fluid temperature, $T_{ref}$is the reference temperature and α is the thermal diffusivity of the fluid.

The RANS approach attempts to directly solve the mean flow properties by employing a Reynolds decompositions of each flow variable $\phi\left(\mathbf{x},t\right)$ into its mean component $\bar{\phi}\left(\mathbf{x},t\right)$ and associated turbulent fluctuations $\phi'\left(\mathbf{x},t\right)$ which describe the chaotic behaviour of the flow. The scalar ϕ quantity denotes the individual velocity components, u_i with $i = x, y, z$, the pressure and the temperature. By substituting this decomposition into Equation 1 and averaging over time, the Unstable Reynolds-average Navier-Stokes (URANS) equations are obtained:

$$\begin{cases} \dfrac{\partial \overline{\mathbf{u}}}{\partial t} + (\overline{\mathbf{u}} \cdot \nabla)\overline{\mathbf{u}} - \nabla \cdot (\nu \nabla \overline{\mathbf{u}}) = -\dfrac{1}{\rho}\nabla \overline{p} - \mathbf{g}\beta(\overline{T} - T_{ref}) - \nabla \cdot (\overline{\mathbf{u}'\mathbf{u}'}) \\ \nabla \cdot \overline{\mathbf{u}} = 0 \\ \dfrac{\partial \overline{T}}{\partial t} + \overline{\mathbf{u}} \cdot (\nabla \overline{T}) = -\nabla \cdot (-\alpha \nabla \overline{T}) - \nabla \cdot (\overline{\mathbf{u}'T'}) \end{cases} \tag{2}$$

with 9 additional terms represented by the Reynolds stress tensor $-\overline{\mathbf{u}'\mathbf{u}'}$ and the turbulent heat transfer $-\overline{\mathbf{u}'T'}$, corresponding to the mean effects of turbulence transfer of momentum and temperature, respectively. In order to close the problem it is possible to rely on different turbulence models available for URANS. In the current study, the linear eddy viscosity models $k-\varepsilon$ [8] and $k-\omega$ SST (Shear-Stress Transport model) [9], based on the turbulent viscosity hypothesis introduced by Boussinesq, the non-linear eddy viscosity model Shih quadratic $k-\varepsilon$ [10] which relates the turbulent stresses algebraically to the rate of strain and includes higher order quadratic terms, and the Reynolds Stress transport Model (RSM) of Speziale, Sarkar and Gatski (SSG) [11] based on transport equations for all components of the Reynolds stress tensor using differential transport equations, are considered.

In the finite-volume open-source code OpenFOAM 6.0, the system of equations 2 is solved by using the segregate PISO (Pressure Implicit with Splitting of Operators) method. The Euler scheme is adopted for the transient simulation. The convection terms are discretized by Gauss Upwind scheme and the diffusion term is solved by Gauss linear uncorrected scheme.

3.3 Properties and conditions of the LBE working fluid

In the present work, temperature-dependent dynamic viscosity, thermal conductivity and specific heat of LBE are adopted referring to [12]. The density is considered constant with respect to temperature and equal to 10'427 kg m^{-3}. A constant turbulent Prandtl number of LBE equal to 1.63 is considered, evaluated from the correlation proposed by [13]. The initial and boundary conditions are reported in Table 2. The inlet mass flow rate is set by MYRRHA design to 0.08 kg s^{-1} with an inlet temperature equal to 220°C. The Reynolds and Prandtl numbers at the inlet correspond to 41'000 and 0.031, respectively. For the outlet boundary condition the model uses an outflow condition (zero velocity gradient and fixed pressure value). Here Reynolds and Prandtl numbers reach the values of 56'000 and 0.019, respectively. At the wall (cladding outer surface), a thermal flux profile is imposed on the basis of the data provided by SCK CEN within the PATRICIA Project [14]. On the other domain walls, symmetric boundary conditions are exerted (Figure 2) as in [15].

4 NUMERICAL RESULTS

This section discusses the results obtained with the URANS turbulence models adopted in OpenFOAM for the numerical setup shown in previous paragraphs. In the first part, the discussion concerns the key thermal-hydraulic parameters predicted by the different turbulence

[2] φ is an arbitrary variable that refers to turbulent kinetic energy, dissipation rate and specific dissipation rate.

Table 2: Initial and boundary conditions of the OpenFOAM simulations.

	Inlet	Outlet	Wall
Velocity	flow rate $0.08\ kg\ s^{-1}$	Zero-gradient	No-slip
	and density $10'427\ kg\ m^{-3}$		$\mathbf{u} = 0$
Temperature	Fixed value $T = 220°C$	Adiabatic $\partial T/\partial n = 0$	Sinusoidal gradient
Pressure	Zero-gradient	Fixed value $p = 0\ bar$	Zero-gradient
Turbulence	Free-stream values	Outflow: $\partial\varphi/\partial n = 0$	Low-Reynolds
		Backflow: $\varphi \cdot n = 0$[2]	number approach

models, such as the sub-channel temperature field, velocity field, pressure drops, and Nusselt number. In the second part, qualitatively comparison of the flow domain cross sections is performed, in order to assess the discrepancy between isotropic ($k-\varepsilon$ and $k-\omega$ SST) and anisotropic (Shih quadratic $k-\varepsilon$ and SSG) turbulence models.

4.1 Model comparison

Figure 3 demonstrates that the minimum sub-channel length required to obtain a fully developed velocity field with LBE as working fluid correspond to 100mm, as stated in 3.1.

From the comparison of the cladding outer temperature evaluated with the turbulence models in Figure 4, only slight deviations emerge. The maximum differences is attested to be of 3°C between SSG and Shih quadratic $k-\varepsilon$ models. The safety limit of 400°C imposed on the coolant temperature during MYRRHA normal operation, to avoid excessive outer cladding corrosion, is respected in all the considered simulation cases. The slight discrepancies between the heat transfer mechanism evaluated by the different URANS models is also visible in Figure 5. Moreover, comparable trends can be observed between the Nusselt number obtained from the computational results and the Ushakov correlation (Table 3), while slightly higher values are predicted by the $k-\varepsilon$ and the Shih Quadratic $k-\varepsilon$ models[3]. The strong changes in Nusselt number observed near the inlet can be attributed to the development of temperature field along the length of the sub-channel, as also attested in [16].

It should be noted the main characteristic of liquid metals, namely that the thermal boundary layer, highlighted in Figure 6, is thicker than that of the hydraulic boundary layer, highlighted in Figure 3. Consequently a larger domain length is needed to obtain a fully developed temperature profile than that of the velocity profile.

In Table 4 the output values of some thermal-hydraulic parameters are collected. The pressure drops predicted by the various models are similar. The number of iterations required to obtain a converged solution is also reported. The numerical solutions were considered to be converged when the initial residuals decrease by five orders of magnitude and reach a value that do not change by performing more iterations.

Table 3: Selected literature correlations for LBE heat transfer and hexagonal lattice, where x is the pitch-to-diameter ratio.

Reference	Correlations	Range
Ushakov et al. [17]	$Nu = 7.55x - 20x^{-13} + 0.041x^{-2}Pe^{(0.56+0.19x)}$[4]	$1 \leq Pe \leq 4000$
		$1.3 \leq x \leq 2.0$
Subbotin et al. [18]	$Nu = 0.58\left(2\sqrt{3}x^2/\pi - 1\right)^{0.55} Pe^{0.45}$	$80 \leq Pe \leq 4000$
		$1.1 \leq x \leq 1.5$

[3] The Peclet number experiences in the MYRRHA IPS sub-channel ranges from 1283 (inlet) to 1081 (outlet).

[4] The extended formula able to cover the range $1.0 \leq x \leq 2.0$ is considered in this work but not reported here.

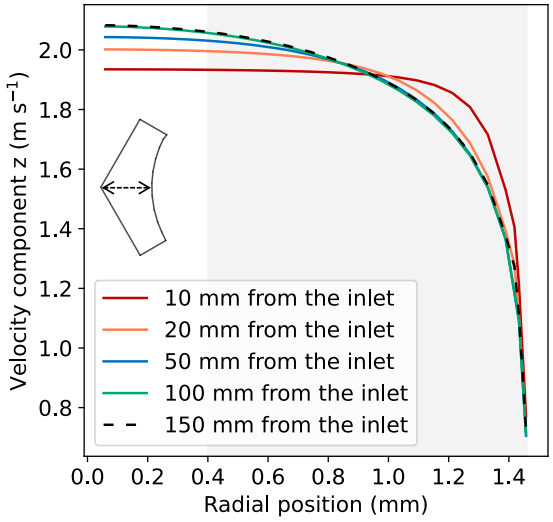

Figure 3: Velocity development along the length of the sub-channel. Results obtained with the $k-\omega$ SST turbulence model. In grey, the extension of the hydraulic boundary layer is highlighted.

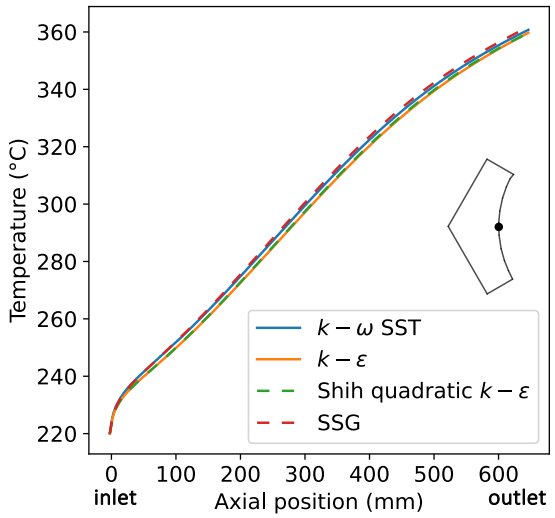

Figure 4: Comparison of the cladding outer temperature evaluated with different turbulence models.

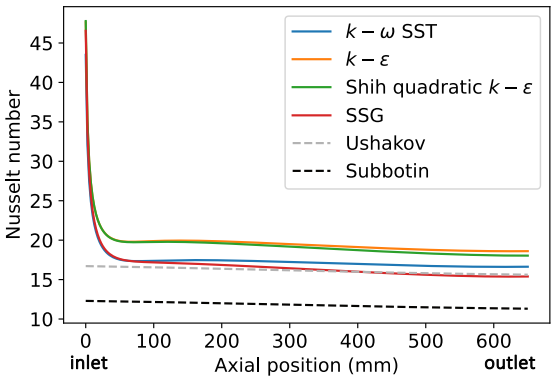

Figure 5: Comparison of the Nusselt number evaluated with different turbulence models and with the empirical correlations for LBE reported in Table 3 along the length of the sub-channel.

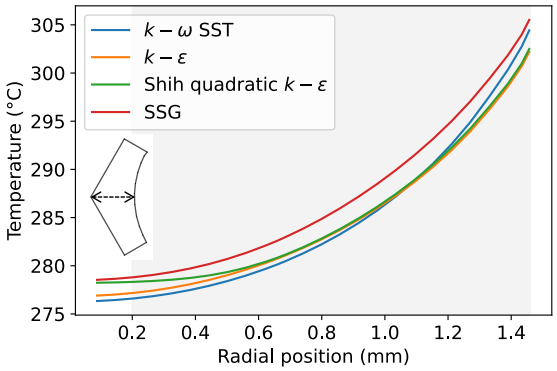

Figure 6: Radial temperature profile evaluated at midplane of the sub-channel for the different URANS models. In grey, the extension of the thermal boundary layer is highlighted.

Table 4: Turbulence model prediction of the mean eddy kinematic viscosity and eddy thermal diffusivity, and the total pressure drops (gravitational and frictional). The number of iterations required is also reported.

	ν_T $(10^{-5}\ \frac{m^2}{s})$	α_T $(10^{-5}\ \frac{m^2}{s})$	Total pressure drops (bar)	Iterations
$k-\varepsilon$	1.06	0.65	1.85	13'000
$k-\omega$ SST	0.90	0.55	1.22	12'000
Shih Quadratic $k-\varepsilon$	1.70	1.05	1.80	15'000
SSG	1.16	0.71	1.65	14'000

4.2 Secondary flow pattern comparison

In Figure 7 it is possible to see that both the $k-\varepsilon$ and the $k-\omega$ SST model are not able to predict the secondary flow formation on either side of the domain cross section, whereas the Shih quadratic $k-\varepsilon$ and the SSG models provide this capability as already shown in [19]. This is due to the ability of these models to account for anisotropic effects. The highest velocity of secondary motion is predicted by SSG Reynolds stress model and is around 1.63% of the mean axial velocity. Contrary to what concluded in [15], the influence of flow anisotropy do not have a strong impact on heat transport (Figure 4, 5 and 6).

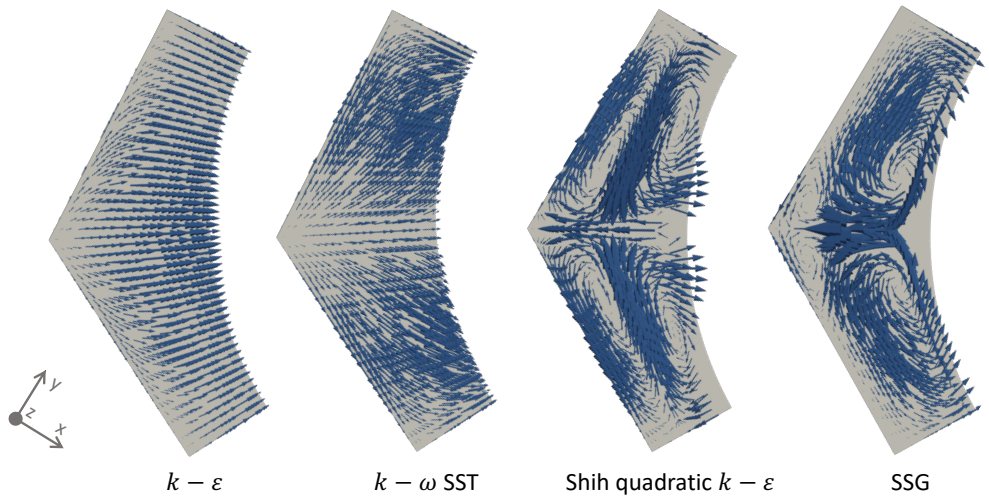

Figure 7: Secondary flow vectors on the cross-sectional midplane of the sub-channel predicted by the isotropic ($k-\varepsilon$ and $k-\omega$ SST) and anisotropic (Shih quadratic $k-\varepsilon$ and SSG) turbulence models.

5 CONCLUSIONS

The aim of this work is to provide detailed insight into the physics of the LBE flow and the associated heat transfer in the interior sub-channel of the MYRRHA IPS sub-assembly during normal operation by performing different URANS simulations in the OpenFOAM 6.0 fluid dynamics software. The comparison of the applied turbulence models revealed that, while the heat transfer mechanism is similar, the anisotropic type models (Shih quadratic $k-\varepsilon$ and SSG) clearly emerge as the higher-accuracy models to predict secondary flow pattern. A better prediction of these coherent structures would allow for a more accurate understanding of mixing between flows in neighbouring sub-channels.

The analysis carried out in this work has also been done with the perspective of enhance the predictive capabilities of the fuel performance code TRANSURANUS [20] by providing more specific and reliable thermal-hydraulics boundary conditions (e.g., cladding outer temperature and pressure drops), to support the design optimization and safety assessment of the MYRRHA fuel pin thermo-mechanical behaviour.

ACKNOWLEDGMENTS

The work described in this paper has received funding from the Euratom research and training programme 2019-2020 under grant agreement No 945077 (PATRICIA Project). I would like to thank my PhD supervisors Prof. Lelio Luzzi and Dr. Davide

Pizzocri for giving me the opportunity to attend this conference.

REFERENCES

[1] V. Sobolev, “Database of thermophysical properties of liquid metal coolants for GEN-IV”. *SCIENTIFIC REPORT SCK•CEN-BLG-1069*, 2011, https://43095088.pdf.

[2] H.A. Abderrahim, D. De Bruyn, M. Dierckx, R. Fernandez, L. Popescu, M. Schyns, A. Stankovskiy, G. Van den Eynde, D. Vandeplassche, “Myrrha accelerator driven system programme: recent progress and perspectives”. pp. 29-42, 2019, doi: doi.org/10.26583/npe.2019.2.03.

[3] H. Kawamura, H. Abe, Y. Matsuo, “DNS of turbulent heat transfer in channel flow with respect to Reynolds and Prandtl number effects”, *Int. J. Heat Fluid*, vol. 20, pp. 196–207, 1999, doi: 10.1016/S0142-727X(99)00014-4.

[4] G. Grötzbach, “Challenges in low-Prandtl number heat transfer simulation and modelling”, *Nucl. Eng. Des.*, vol. 264, pp. 41-55, 2013, doi: 10.1016/j.nucengdes.2012.09.039.

[5] OpenFOAM version 6.0, 2018, website: https://doc.cfd.direct/openfoam/user-guide-v6/.

[6] L. Fiorito, A. Hernandez-Solis, and P. Romojaro, “Homogenized neutronics model of MYRRHA design revision 1.8”. *Report for SANDA H2020 Project*, 2021.

[7] G. Van Den Eynde, E. Malambu, A. Stankovskiy, R. Fernandez, and P. Baeten, “An updated core design for the multi-purpose irradiation facility MYRRHA”. *J. Nucl. Sci. Technol.*, vol. 52, pp 1053-1057, 2015, doi: 10.1080/00223131.2015.1026860.

[8] B.E. Launder and D.B. Spalding, “The numerical computation of turbulent flows”, *Computer methods in applied mechanics and engineering*, vol. 3, pp. 269–289, 1974, doi: 10.1016/0045-7825(74)90029-2.

[9] F. R. Menter, “Two-equation eddy-viscosity turbulence models for engineering applications”, *AIAA Journal*, vol. 32, no. 8, 1994, doi: 10.2514/3.12149.

[10] T. Shih, J. Zhu, and J. L. Lumley, “A Realizable Reynolds Stress Algebraic Equation Model”, *NASA Tech. Memo*, vol. 16596, 1993, doi: 10.1016/0045-7825(95)00796-4.

[11] C. G. Speziale, S. Sarkar, and T. B. Gatski, “Modelling the pressure-strain correlation of turbulence : An invariant dynamical systems approach”, *J. Fluid. Mech.*, vol. 227, 1991, doi: 10.1017/S0022112091000101.

[12] NEA (2015), ”Handbook on Lead-bismuth Eutectic Alloy and Lead Properties, Materials Compatibility, Thermal-hydraulics and Technologies”, 2015 Edition, OECD Publishing, Paris, https://www.oecd-nea.org.

[13] X. Huang, B. Pang, X. Chai, and Y. Yin, “Proposal of a turbulent Prandtl number model for Reynolds-averaged Navier–Stokes approach on the modeling of turbulent heat transfer of low-Prandtl number liquid metal”.*Front. in En. Res.*, 2022, vol. 10, doi: 10.3389/fenrg.2022.928693.

[14] European Union’s Horizon 2020 Research and Innovation programme, “PATRICIA - Partitioning And Transmuter Research Initiative in a Collaborative Innovation Action”, 2020, https://patricia-h2020.eu.

[15] E. Baglietto and H. Ninokata, “Selection of an appropriate turbulence modeling in a CFD code for an ultra-long life core for the ‘IRIS’ reactor”. *GENES4/ANP2003*, Sep. 15-19, 2003, Kyoto, Japan, https://1153-final.pdf.

[16] L. Chandra, F. Roelofs, M. Houkema, B. Jonker, “A stepwise development and validation of a RANS based CFD modelling approach for the hydraulic and thermal-hydraulic analyses of liquid metal flow in a fuel assembly”, *Nucl. Eng. Des.*, vol. 230, pp. 1988-2003, 2009, doi: 10.1016/j.nucengdes.2009.05.022.

[17] Ushakov, P. A., Zhukov, A. V., and Matyukhin, “Heat transfer to liquid metals in regular arrays of fuel elements”, *High Temperature*, 15(5), 1977, http://mi.mathnet.ru/tvt7257.

[18] Subbotin, V. I., Ushakov, P. A., Kirillov, P. L., Ibragimov, M. H., Ivanovski, M. N., Nomofilov, E. M., Ovechkin, D. M., Sorokin, L. N., and Sorokin, V. P, “Heat transfer in elements of reactors with a liquid metal coolant”, *Proceedings of the 3rd International Conference on Peaceful Use of Nuclear Energy*, 8, 192–200, 1965.

[19] X. Cheng and N.I. Tak, “CFD analysis of thermal–hydraulic behavior of heavy liquid metals in sub-channels”, *Nuc. Eng. Des.*, vol. 236, pp 1874-1885, Sept. 2006, doi: 10.1016/j.nucengdes.2006.02.001.

[20] K. Lassmann“URANUS - A computer programme for the thermal and mechanical analysis of the fuel rods in a nuclear reactor”, *Nuc. Eng. Des.*, vol. 45, 1978, doi: 10.1016/0029-5493(78)90225-X.